Functional Materials 11, No.1 (2004)

Radiation detector development in KAERI

Yong Kyun Kim, Se Hwan Park, Jang Ho Ha, Woo Gyo Lee, Seok Boong Hong, Chong Eun Chung

Korea Atomic Energy Research Institute, 150 Deokjin-dong, Yuseong, Daejeon 305-600, Korea

The radiation detector research group in KAERI has developed two types of gas-filled radiation detectors, a Gas Electron Multiplier (GEM) and an ion chamber. The double GEM and triple GEM were fabricated and operated in several gas mixtures to obtain large gains of about $5 \cdot 10^4$ and $6 \cdot 10^5$, respectively, in the Ar/Isobutane mixture. For the application to GEM Photo Multiplier (GPM), the ion feedback dependency of the double GEM was carefully measured according to the drift electric field, the transfer field, the asymmetry of the GEM voltage, and the effective gain in various gas mixtures. The ion feedback depends significantly on the drift field and the effective gain, however it is almost independent of the gas mixture. A model of ion feedback in a double GEM structure was derived, and its prediction was compared with the experiment. The optimum value of the transfer field and the dependency of the collection current with respect to the drift, transfer, and collection field strengths for the GEM voltage sharing in the double GEM were measured. An air-filled ion chamber was designed and fabricated as a prototype of the beam loss monitor for the high power accelerator. The collection efficiency and stability of the ion chamber with respect to the different radii of anode electrode were measured.

Исследовательской группой KAERI по радиационным детекторам разработаны два типа газонаполненных радиационных детекторов — газовый электронный умножитель (GEM) и ионизационая камера. Изготовлены двойной GEM и тройной GEM и испытаны с применением различных газовых смесей; высокие коэффициенты умножения (соответственно $5 \cdot 10^4$ и $6 \cdot 10^5$) получены в смеси аргона с изобутаном. С целью применения GEM была тщательно измерена зависимость ионной обратной связи для двойного GEM от дрейфового электрического поля, транспортного поля, асимметрии напряжения на GEM и эффективного коэффициента умножения в различных газовых смесях. Ионная обратная связь существенно зависит от дрейфового поля и эффективного коэффициента умножения, однако почти не зависит от используемой газовой смеси. Разработана модель ионной обратной связи для двойного GEM, и сделанные на ее основе прогнозы сопоставлены с экспериментальными результатами. Измерено оптимальное значение транспортного поля и зависимости для коллекторного тока от напряженности дрейфового, транспортного и коллекторного полей для распределения напряжения в двойном GEM. Разработана и изготовлена воздушная ионизационная камера в качестве прототипа монитора потери пучка в ускорителе высокой мощности. Измерены эффективность сбора и стабильность работы ионизационной камеры при различных радиусах анодного электрода.

All single stage micro-pattern gas detectors suffer from discharge and fatal sparking damage as the result of the huge amount of primary electrons that are generated by the heavily ionizing particles passing the detector [1]. A new concept of a gas avalanche detector was introduced by Sauli [2] with a Gas Electron Multiplier (GEM) in 1997. Considerable progress has been made motivated by the growing interest in the application of GEM. GEM is superior to other gas detectors in the respect of a high counting rate, excellent spatial resolution, good imaging capability, operative in a magnetic field, large sensitive area, flexible geometry, and low cost [3]. In KAERI, GEM was operated coupled with MWPC and MSGC, and the charge sharing and electron transfer process were examined [4, 5].

Another interesting application of GEM is the GEM based photo multiplier. The broader use of a gas photon detector, especially in a commercial system, has been hindered by the necessity of permanent gas flushing. Sealed gas detectors usually age very fast in standard gas mixtures, and the operation in a noble gas can prevent the problem. However, the gain in a noble gas filled detector is usually very low due to the photon and ion mediated secondary process [6]. Since the electron avalanche in GEM is confined to the hole, GEM has then advantage of being operated with a high gain in pure noble gas [7].

The GEM photomultiplier has been investigated intensively at present [3], however the ion feedback has to be reduced to prevent photocathode degradation from the ion impact. Ion feedback was measured previously in single and multiple GEM structures [8, 9]. One of the interesting features in the previous studies was that the ion feedback ratio (the ratio of the cathode-to-anode current) was independent of the gas and pressure for a given gain even though the applied voltages across the GEM in the various gas conditions were not the same. It means that the charged particle diffusion, which is the function of pressure, gas, and electric field, does not affect the ion feedback. However, only a few kinds of gas mixtures were used in the previous experiment [8], it is necessary to confirm the gas effect on the ion feedback. Also, it would be helpful to understand the ion feedback effect systematically for the gas detector development with GEM.

In our experiment, the ion feedback effect in a multi-GEM structure was studied extensively in various gas conditions using a double GEM structure. And the anode signal was recorded directly through the bottom of the second GEM. It helps to understand the ion feedback phenomena using a small number of parameters. An ion feedback model was made for our GEM structure. The effects of the drift field, the asymmetry of the applied voltage across the GEM, and the gain on the ion feedback can be explained with the charge transfer parameters of a single GEM.

Fig. 1 shows the experimental setup of a double GEM detector. The physics of a multi GEM structure can be described with a few parameters [8], which are from the charge transfer mechanism in single GEM. In a single GEM foil, collection efficiency, gain, and extraction efficiency will determine the charge transfer. The collection efficiency is the probability of a charged particle in the drift region between the drift plate and GEM1 to be transferred into a GEM hole. The gain is the factor by which the number of electrons is multiplied by a gas avalanche inside the GEM hole. The extraction efficiency is the fraction of charged particles to be extracted from the GEM holes into the transfer volume between the GEM1 and GEM2.

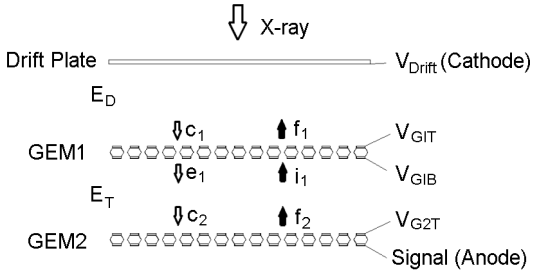

Fig. 1. Schematics of a double GEM detector. Collection efficiencies and extraction efficiencies of electrons (c_i and e_i) and ions (i_i and f_i) are also noted, which are for model calculations.

Previous measurements and numerical simulations on the charge transfer in the single GEM were performed to understand the charge transfer parameters [10]. The gain is determined by the mean electric field inside the GEM hole, E_{hole}. That is, the E_{hole} of GEM1 in Fig. 1 is a linear combination of E_D, E_T, and ΔV_{GEM}:

$$E_{hole} = a\Delta V_{GEM} + b(E_D + E_T), \qquad (1)$$

where a and b depend on the GEM geometry. The collection efficiency is a function of the field ratio E_D/E_{hole}. The collection efficiency decreases in a high drift field due to the defocusing of the field lines above the GEM. The collection efficiency of the electron and ion shows a sharp decrease when the E_D/E_{hole} approaches zero. It is due to the recombination of charge pairs at a very low drift velocity. The extraction efficiency is a function of E_T/E_{hole}. The extraction efficiency increases with E_T/E_{hole}, because more charged particles can be extracted from the lower side of the GEM foil in larger E_T/E_{hole}.

Our measurement of the ion feedback effect in the multi GEM can be explained from the charge transfer parameters in a single GEM. Let us say that the electron collection efficiency into the GEM hole c_i, the real gain of a GEM g_i, electron extraction efficiency from the GEM hole e_i. The

ion extraction efficiency from the GEM hole is f_i, and the ion collection efficiency into the GEM hole is i_i. Each parameter is shown in Fig. 1.

Then the effective gain, G, in our double GEM structure is

$$G = c_1 g_1 e_1 c_2 g_2. \quad (2)$$

The ion feedback fraction to the cathode, I_D, is

$$I_D = c_1 g_1 f_1 + c_1 g_1 e_1 c_2 g_2 f_2 i_1 f_1. \quad (3)$$

The first term is from the ions generated in GEM1, and the second term is from the ions generated in GEM2. Then the ion feedback ratio (I_D/G) can be expressed as

$$I_D/G = f_1(i_1 f_2 + 1/e_1 c_2 g_2) = \quad (4)$$
$$= f_1(i_1 f_2 + c_1 g_1/G).$$

The experimental setup shown in Fig. 1 was similar to that used in [4, 5]. Two GEM foils (Kapton thickness 50 μm, hole diameter 60 μm the metal side, and hole pitch 100 μm) of a 10×10 cm^2 active area each, were mounted in a cascade inside a stainless-steel chamber. The GEM foils were made at CERN. The drift plate, which was made of aluminized Mylar, was placed above GEM1. The drift gap between the drift plate and GEM1, and the transfer gap between GEM1 and GEM2 were 3 mm and 2 mm, respectively. The 5.9 keV X-rays from ^{55}Fe were irradiated through a 0.5 mm thick Be window, and the anode signal was measured directly through the bottom electrode of GEM2. The anode and cathode signals were measured in a current mode. Each electrode (V_{G1T}, V_{G1B}, V_{G2T}, and V_{Drift}) was connected to an individual channel of a power supply, allowing the flexible setting of the electric fields in the two gaps and voltages across the GEM surfaces.

Effective gain of the detector was defined as the anode current divided by the primary ionization current, which was measured when the drift gap was operated in an ionization mode with $\Delta V_{GEM} = 0$. The ion feedback ratio was defined as the cathode current divided by the anode current. Highly pure (99.999 %) $Ar + CO_2$ or $Ar + N_2$ flew through the chamber, and the gas mixing ratio was changed to get the influence of gas on the ion feedback. In the case of the triple GEM, the drift electric field E_D was fixed at 2 kV/cm, the transfer electric field E_T was varied to 1, 3, and 5 kV/cm. A large gain of about $6 \cdot 10^5$ was

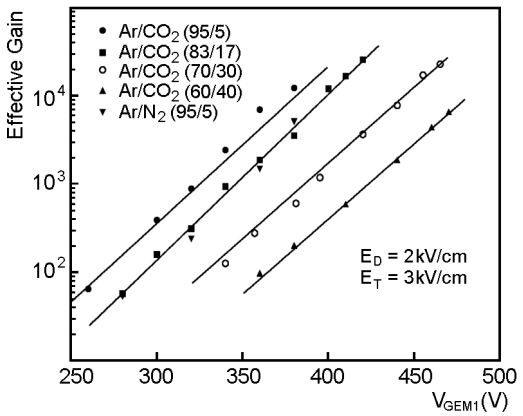

Fig. 2. Effective gain as a function of voltage across the GEM. E_D was kept constant.

obtained for the Ar/Isobutane mixture. For the double GEM, E_D and E_T were fixed at 2 kV/cm and 3 kV/cm, respectively. We biased the same $\Delta V_{GEM's}$ in GEM1 and GEM2. The effective gain follows the exponential behavior up to a high ΔV_{GEM}. Fig. 2 shows the voltage-effective gain characteristics in various gas mixtures, where the lines are the exponential function of the voltage across the GEM (ΔV_{GEM}).

The effects of the effective gain and gas mixing ratio of the various gases on the ion feedback ratio are shown in Fig. 3. The ion feedback ratio for a given effective gain was measured with the various gas mixtures of Ar/CO_2 or Ar/N_2. The ion feedback ratio decreased with the effective gain, and it was almost independent of the gas mixing ratio, which was consistent with the previous result [8]. It means the diffusion of charged particles does not affect the ion feedback.

Fig. 4 shows the effect of E_D on the ion feedback. The same voltages were biased across GEM1 and GEM2. E_T = 3 kV/cm and ΔV_{GEM} in each gas mixture was kept constant to make the effective gain 10^3. The ion feedback ratio increased almost linearly with E_D. But the effective gain was not so sensitive to E_D.

Fig. 5 shows the effect of E_T in various gas mixtures. The voltage across GEM1 was also equal to the voltage across GEM2. The data was obtained with a fixed E_D (2 kV/cm) and ΔV_{GEM}. Effective gain increased with E_T, and the ion feedback ratio decreased slowly with E_T in the high E_T region. Fig. 6 shows the effect of E_T in various gas mixtures. The voltage across GEM1 was also equal to the voltage across GEM2. The data was obtained with a fixed E_D (2 kV/cm) and ΔV_{GEM}. Effective gain in-

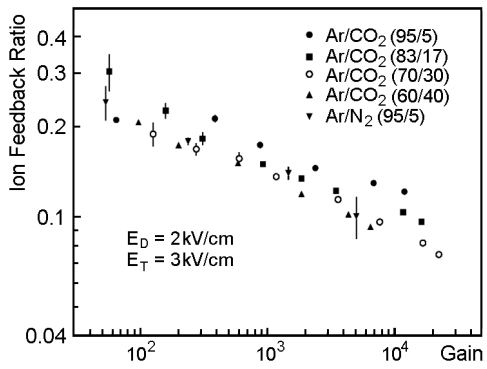

Fig. 3. Ion feedback ratio as a function of effective gain. E_D and E_T were kept constant.

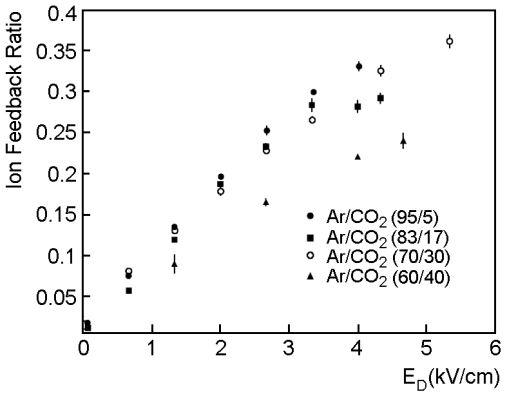

Fig. 4. Ion feedback ratio vs. E_D.

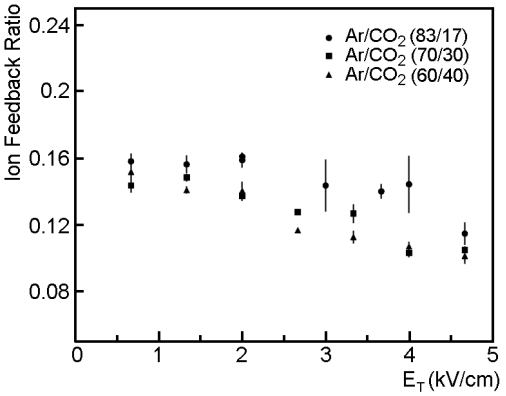

Fig. 5. Ion feedback ratio vs. E_T.

creased with E_T, and the ion feedback ratio decreased slowly in the high E_T region.

The effect of the asymmetry of $\Delta V_{GEM's}$ on the ion feedback ratio was also measured, which is shown in Fig. 6. Only the voltages across GEM1 and GEM2 were changed. We increased ΔV_{GEM} of GEM1 and ΔV_{GEM} of GEM2 was decreased to keep the same effective gain of 10^3. As the voltage across GEM1 became higher, the ion feedback ratio increased.

Since G is almost independent of E_D in our measurement, it is assumed that b of Eq.1 can be negligible. Then E_D and E_T do not affect g_i. The effect of E_D on the ion feedback ratio can be understood from Eq.4. E_D can affect f_1, and f_1 increases with E_D [10], which is consistent with Fig. 4.

The effect of the asymmetry in $\Delta V_{GEM's}$ on the ion feedback ratio follows from the model. Eq.4 predicts that if the effective gain (G) remains the same, the ion feedback ratio will increase with g_1, which is consistent with Fig. 6. The discrepancies of the ion feedback ratio with respect to the gas mixture in Fig. 6 comes from the fact that g_1's are different in various gas mixtures even if the same ΔV_{GEM} is applied, which is shown in Fig. 2.

The effective gain dependency on the ion feedback ratio is also from Eq.4. ΔV_{GEM} can affect all the parameters in Eq.4. However, the effect of ΔV_{GEM} on g_i is much larger than the effect on the other parameters. Therefore, one can assume all the parameters are constant except g_i if only ΔV_{GEM} is varied. Since g_1 is equal to g_2 in our measurement, one can get

$$I_D/G = a + b/G^{1/2}, \quad (5)$$

where a is $f_1 i_1 f_2$, and b is $f_1(c_1/e_1c_2)^{1/2}$.

We can make a fit to the measurement using Eq.5, which is shown in Fig. 7. The lines are from the least square fitting, and the circles are from the measurement. The model can explain the effective gain dependency of the ion feedback ratio except in the higher gain region. That is, the measured data is smaller than the model prediction. As pointed out by Bondar [8], it could be related to the avalanche extension effect in the GEM. Since the positive ions are produced outside the GEM hole in a higher gain, it has more chance to drift to the bottom of the GEM rather than entering the hole.

We made a model prediction for our measurement, and the ion feedback ratio can be explained by the collection efficiency, gain, and extraction efficiency in a single GEM. The effective gain dependency was well reproduced by the model prediction except in a higher gain, which could be understood by the avalanche extension. Also the model can explain the ion feedback effect of the asymmetry of ΔV_{GEM}. With our study, one can predict the ion feedback effect in a multi GEM structure from the

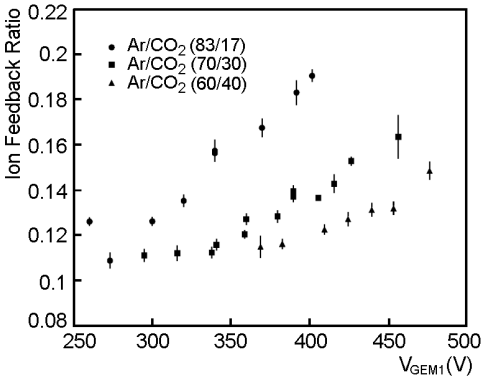

Fig. 6. Effect of asymmetry of ΔV_{GEM} on the ion feedback ratio. Effective gain was set constant at 10^3 during the measurement. ΔV_{GEM1} means the voltage across GEM1.

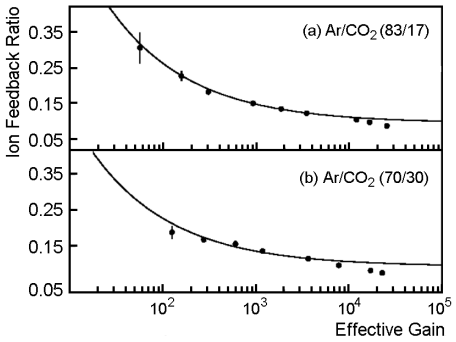

Fig. 7. The phenomenological formula about the effective gain dependency on the ion feedback was fitted to the measurement. The lines are the fitting result, and the circles are the data.

charge transfer parameters in a single GEM, which could be helpful for further research on a GEM photomultiplier and TPC.

The PEFT (Proton Engineering Frontier Project) is to build an 100 MeV, 20 mA proton linear accelerator in Korea. An accelerator facility with such an high intensity beam needs the BLM system for the primary diagnostic tool for tuning and preventing excess activation and equipment damage. The detector of BLM has to satisfy many requirements. The gain of the detector has to be stable with time. The components of it should be tolerant to the radiation. If the detector is replaced with new one, the gain of it can be recalibrated easily. Ion chamber can satisfy such requirements, and a number of accelerator facilities select the ion chamber as the BLM detector [11]. We designed an ion chamber for BLM. The ion chamber is cylindrical shape, and argon is filled inside the chamber. Before the parameters of the ion chamber are determined, we fabricated a prototype ion chamber. Air was filled inside the chamber, and the response of the ion chamber was measured. With these data, we can design the BLM ion chamber specifically.

A prototype ion chamber for the BLM was fabricated, and the saturation curve of the ion chambers was measured. The prototype ion chamber was constructed of two concentric cylinders filled with air as shown in Fig. 1. The cylinders were 210 mm long and made of 2-mm thick aluminum. The diameter of outer electrode was 38 mm, and three different diameter inner electrodes were made (Type 1:diameter of 6 mm, Type 2:16 mm, and Type 3:25 mm). The inner electrode was hollow and filled with air inside. Guard electrode, which could reduce the leakage current of the collecting electrode, was made of copper, and it was placed in the middle of the inner electrode and the outer electrode. Teflon insulators were placed between electrodes. The ion chamber was housed inside the 2-mm thick aluminum cylinder. Two MHV connectors were mounted for signal collection and high voltage biasing. These connector structure could help the easy daisy chaining. Fig. 8 shows the prototype ion chamber.

The saturation curve of the ion chamber was measured. 60 keV γ-rays from ^{241}Am were incident perpendicular to the cylinder surface, which make the dose rate of 2 mSv/h inside the ion chamber. High voltage was biased on one connector with ORTEC high voltage supplier Model 660, and the collecting signal was recorded from the other connector with Keithley Electrometer Model 6517A. The high voltage was biased on the outer electrode, and the signal was measured on the inner electrode. After that the high voltage was biased on the inner electrode and the signal was recorded on the outer electrode. The polarity of the bias was also reversed. It could give the influence of the bias polarity on the ion chamber operation. Since we measured the saturation curve with three different types of inner electrodes, we could also determine the adequate diameter of the inner electrode.

The collection efficiency f of an ion chamber at a given bias voltage V can be defined as the ratio of the measured current to the ideal saturation current. The equations for describing f have been known since Thomson described them in 1899 [12]. However, they have not been solved in

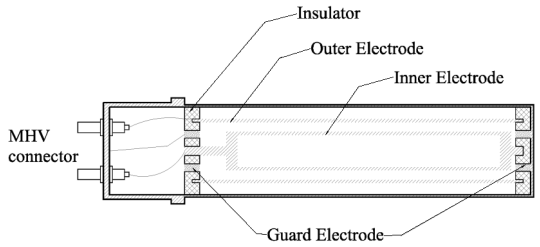

Fig. 8. The prototype ion chamber.

closed form. Approximated result, which gives a good fit for $f \geq 0.7$, is [13]

$$f = 1/(1 + \xi^2), \tag{6}$$

where

$$\xi^2 = \frac{\alpha}{6ek_1k_2}\frac{d^2}{V^2}\frac{Q_\infty}{vol}. \tag{7}$$

Here, e is the electron charge, k_1 the electron mobility, k_2 the ion mobility, d the equivalent gap, Q_∞ the saturation charge at infinite applied voltage, vol the collecting volume of the ion chamber, and α is the first Townsend recombination coefficient. d for the cylindrical ion chamber can be expressed as

$$d = (a - b)\left[\frac{a + b}{a - b}\,\frac{\ln(a/b)}{2}\right]^{1/2}, \tag{8}$$

where a is the radius of outer electrode, and b is the radius of inner electrode. From above equations, we can see that the signal can be saturated easily in lower bias voltage as the distance between the outer electrode and the inner electrode gets closer.

The saturation curve of Type II ion chamber is shown in Fig. 9. The curve reaches a flat zone, and the charge multiplication occurs when the voltage is higher than 2000 V. We use three different methods, the inverse voltage method, the two voltage method, and fitting to Eq.6, to obtain the voltage, where f reaches 0.999, for each saturation curve [13]. The line in Fig. 9 is from Eq.6, in which the parameters of Q_∞ and $\alpha/6ek_1k_2$ are taken from the fitting result.

The biased voltages $f = 0.999$, where $f = 0.999$, are obtained from the above three methods. Fig. 10 shows $V_f = 0.999$ in the case of the negative voltage biased on the outer electrode. As one can expect, the measured current can be saturated in lower voltage if the distance between the outer electrode and the inner electrode gets

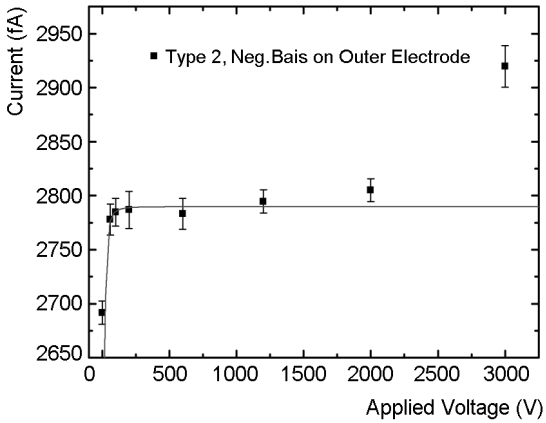

Fig. 9. The saturation curve of the ion chamber type II. The negative voltage was biased on the outer electrode, and the signal was recorded on the inner electrode. The line is from the fitting with the theoretical line.

closer. Three methods give the similar result except the case of $b = 5$ mm. Since the inverse voltage method assumes that the recombination takes place within the track of single particle ionization, it can not give a reliable result.

Because beam loss monitoring system will be placed in the high dose environment, it is better to get the saturation current with lower biased voltage. The ion transit time can be expressed as [14]

$$t = \frac{d^2}{\mu_0 V(P_0/P)}, \tag{9}$$

where μ_0 is the ion mobility, V applied voltage, P_0 atmospheric pressure, and P is the working pressure. If d gets smaller, we can collect ions in shorter time.

However, the field becomes unstable when the inner electrode is too close to the outer electrode. In our measurement with ion chamber Type III (Inner electrode diameter: 25 mm), the signal shows fluctuation above $V = 2000$ V. And, as the inner electrode gets close to the outer electrode, we will get smaller current. From the above consideration, we choose 20 mm for the diameter of inner electrode.

The BLM ion chamber parameters are as follows. The BLM ion chamber will be a aluminum cylindrical shape of 210 mm long. The diameter of outer electrode is 38 mm, and the diameter of the inner electrode is 20 mm, which follows from the measurement with prototype chamber. The thickness of aluminum electrode will be 2 mm, which was from EGSnrc calculation.

The net internal volume of the detector is 103 cm^3. The estimated response is 12 pA/Rad/h. The insulator is made of ceramic. We are underway to test the prototype chamber in high dose rate at KAERI gamma irradiation facility. Also the BLM ion chamber is designed and being fabricated.

Acknowledgement. This work has been carried out under the Nuclear R&D program by the Ministry of Science and Technology of Korea. The authors also wish to acknowledge the support from KOSEF Engineering Research Center program of Innovative Technology Center for Radiation Safety (ITRS) at Hanyang University, Seoul, Korea.

References

1. B.Schmidt, *Nucl. Instr. Meth. A*, **419**, 230 (1998).
2. F.Sauli, *Nucl. Instr. Meth. A*, **386**, 531 (1997).
3. A.Buzulutskov, *Nucl. Instr. Meth. A*, **494**, 148 (2002).
4. S.Han, H.Kang, Y.Kim et al., *J. Kor. Phy. Soci.*, **40**, 820 (2002).
5. S.Han, H.Kang, Y.Kim et al., *J. Kor. Phy. Soci.*, **41**, 674 (2002).
6. A.Buzulutskov, A.Breskin, R.Chechik et al., *Nucl. Instr. Meth. A*, **443**, 164 (2000).
7. A.Buzulutskov, L.Shekhtman, A.Bressan et al., *Nucl. Instr. Meth. A*, **433**, 471 (1999).
8. A.Bondar, A.Buzulutskov, L.Shekhtman, A.Vasiljev, *Nucl. Instr. Meth. A*, 1 (2003).

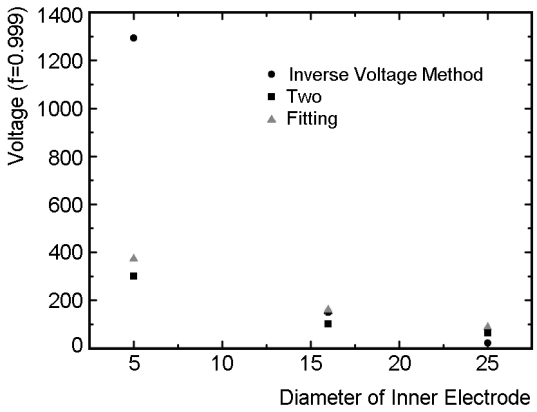

Fig. 10. $V_{f=0.999}$ as a function of the diameter of the inner electrode. The closed circles are from the inverse voltage method, the closed triangles from the two voltage method, and the open squares are from the fitting method. As the diameter of the inner electrode gets larger, $V_{f=0.999}$ gets smaller.

9. S.Bachmann, A.Bressan, L.Ropelewski et al., *Nucl. Instr. Meth. A*, **438**, 376 (1999).
10. M.Killenberg, S.Lotze, J.Mnich et al., *Nucl. Instr. Meth. A*, **498**, 369 (2003).
11. D.Brown, M.A.Plum, A.A.Browmann, R.J.Macek, *Nucl. Instr. Meth. A*, **420**, 494 (1973).
12. J.J.Thomson, *Phil. Mag.*, **47**, 253 (1899).
13. J.W.Boag, The Dosimetry of Ionization Radiation, vol.II, Academic Press, Inc. (1987).
14. R.L.Witkover, D.Gassner, *AIP Conf. Proc.*, **648(1)**, 337 (2002).

Розробка радіаційних детекторів у KAERI

Йонг Кіун Кім, Се Хван Пак, Чжанг Хо Ха, Ву Чжіо Лі, Сеок Бунг Хонг, Чонг Еун Чунг

Дослідницькою групою KAERI з радіаційних детекторів розроблено два типи газонаповнених радіаційних детекторів — газовий електронний помножувач (GEM) та іонізаційна камера. Виготовлені подвійний GEM та потрійний GEM випробувані з застосуванням різних газових сумішей; високі коефіцієнти помноження (відповідно $5{\cdot}10^4$ та $6{\cdot}10^5$) одержано в суміші аргону з ізобутаном. З метою застосування GEM ретельно вимірено залежність іонного зворотного зв'язку для подвійного GEM від дрейфового електричного поля, транспортного поля, асиметрії напруги на GEM та ефективного коефіцієнта помноження в різних газових сумішах. Іонний зворотний зв'язок істотно залежить від дрейфового поля та ефективного коефіцієнта помноження, однак майже не залежить від використаної газової суміші. Розроблена модель іонного зворотного зв'язку для подвійного GEM і прогнози, зроблені на її основі, зіставлені з експериментальними результатами. Виміряно оптимальне значення транспортного поля та залежності для колекторного струму від напруженості дрейфового, транспортного та колекторного полів для розподілу напруги у подвійному GEM. Розроблена та виготовлена повітряна іонізаційна камера як прототип монітора втрати пучка у прискорювача високої потужності. Виміряно ефективність збору та стабільність роботи іонізаційної камери при різних радіусах анодного електрода.